PHYSICS OF PLASMAS **23**, 122507 (2016)

Microturbulence in DIII-D tokamak pedestal. III. Effects of collisions

X. Liao,[1] Z. Lin,[2] I. Holod,[2] Y. Xiao,[3] B. Li,[1,a)] and P. B. Snyder[4]
[1]*Fusion Simulation Center, State Key Laboratory of Nuclear Physics and Technology, School of Physics, Peking University, Beijing 100871, China*
[2]*Department of Physics and Astronomy, University of California, Irvine, California 92697, USA*
[3]*Institute for Fusion Theory and Simulation, Zhejiang University, Hangzhou 310027, China*
[4]*General Atomics, P.O. Box 85608, San Diego, California 92186-5608, USA*

(Received 7 June 2016; accepted 4 August 2016; published online 16 December 2016)

Gyrokinetic simulations of the H-mode pedestal in DIII-D discharge 145701 find that the kinetic ballooning mode (KBM) is the most unstable mode for low toroidal numbers ($n \leq 25$) and that the trapped electron mode (TEM) dominates over the KBM at higher toroidal mode numbers for realistic pressure gradients in the pedestal. Collisions reduce the TEM growth rate but have little effects on the KBM. KBM has the conventional ballooning mode structure peaking at the outer mid-plane, while TEM has an unconventional mode structure peaking at the top and bottom of the poloidal plane. *Published by AIP Publishing*. [http://dx.doi.org/10.1063/1.4972079]

I. INTRODUCTION

Edge instabilities and microturbulence affect the performance of tokamaks in the high confinement (H-mode) operation,[1] which is characterized by steep gradients of density and temperature in the edge region (pedestal). Electrostatic ion/electron temperature gradient-driven instabilities (ITG/ETG)[2–4] and trapped electron mode (TEM),[5–7] electromagnetic instabilities such as kinetic ballooning mode (KBM)[8,9] and micro-tearing modes,[4] and magnetohydrodynamic instabilities such as peeling-ballooning mode (PBM) induced edge localized modes[10–14] can be driven by free energy provided by pedestal gradients. These instabilities may influence pedestal buildup according to the EPED model,[15] which predicts the H-mode pedestal height and width based upon two constraints: the PBM with low to intermediate toroidal mode numbers and the KBM with relatively high toroidal mode numbers. Understanding pedestal physics is crucial for realizing the magnetic confinement fusion energy.

Several simulations using experimental equilibrium profiles have partially verified the EPED model.[9] However, quantitative agreement, especially for the KBM, has not been achieved among simulations and between simulations and experiments.[4] Possible reasons include different equilibria, simulation models, and methods to deal with tokamak geometry in various simulation codes. Recently, linear electrostatic ITG and TEM instabilities exhibiting unconventional mode structures in the steep gradient region of the pedestal have been observed by several simulations.[6,7] It is not clear whether electromagnetic modes such as KBM can exhibit the unconventional mode structure in the steep gradient region of tokamak plasmas. Thus, microinstabilities in the pedestal are not well understood, even for the linear properties. Verification and validation between different codes and with experiments have not been demonstrated. Therefore, comprehensive simulations should be carried out to study the physics of microinstabilities in the pedestal, such as the role of collisions, the unconventional mode structures in the steep gradient region, and the electromagnetic effects.

Using the gyrokinetic toroidal code (GTC),[16–18] earlier simulations[6] of the DIII-D discharge 131997 at time 3011 ms find that the most unstable electrostatic instability in the peak gradient region is the TEM with a growth rate increasing monotonically with the toroidal mode number n. In the electromagnetic simulation,[19] the most unstable mode is the KBM for the dominant poloidal wave number $k_\theta \approx 1\,\mathrm{cm}^{-1}$. For shorter wavelength modes, the dominant instability is the TEM.

In this work, we continue to use GTC to study the linear properties of electromagnetic instabilities in the steep gradient region of the H-mode pedestal in the DIII-D discharge 145701 at time 33 ms, which has more robust KBM signals. We use realistic magnetic geometry from the VMEC[20] equilibrium solver and include collisions in the GTC simulations. We neglect equilibrium flows, which may have an influence on low-n instabilities, and suppress equilibrium current drive, which may destabilize the peeling and kink modes. Compressional magnetic effects are also excluded in the simulations. We find that KBM is the most unstable mode for low toroidal numbers ($n \leq 25$), and TEM dominates over the KBM at higher toroidal mode numbers for realistic pressure gradients in the pedestal. Collisions reduce the TEM growth rate but have little effects on the KBM. KBM has the conventional ballooning mode structure peaking at the outer mid-plane, while TEM has an unconventional mode structure peaking at the top and bottom of the poloidal plane. By increasing the plasma pressure within the ranges inside the pedestal, we find that the low-n mode ($n = 15$) makes a transition from TEM to KBM, while the high-n mode ($n = 40$) is always TEM.

The remainder of this paper is organized as follows: Section II describes the simulation setup. The electromagnetic simulation results are presented in Sec. III. We also discuss collisional effects on these electromagnetic instabilities. Finally, a summary of this work is given in Sec. IV.

[a)] Author to whom correspondence should be addressed. Electronic mail: bli@pku.edu.cn

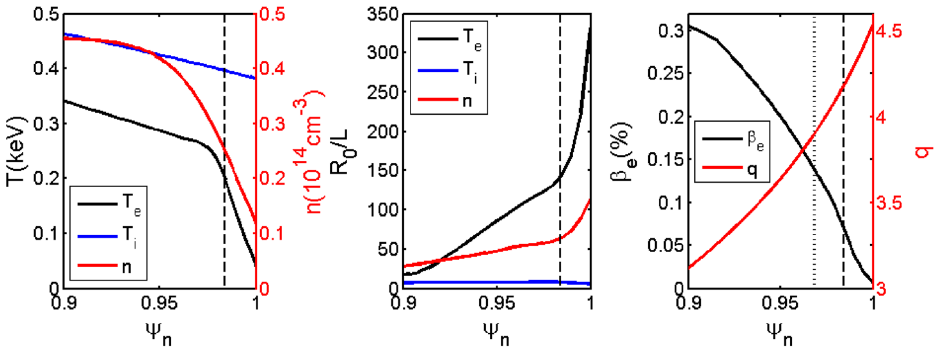

FIG. 1. Plasma profiles in the pedestal region of DIII-D discharge 145701 at time 33 ms as functions of normalized poloidal flux (ψ_n). The panels, from left to right, show normalized temperatures (T_i and T_e), and density ($n_i = n_e$) profiles, inverse temperature and density scale length, β_e values, and safety factor (q). The vertical black dashed line indicates the radial position of the peak gradient region of pedestal and $\beta_e = 0.14\%$ at the dotted line position.

II. SIMULATION SETUP

In GTC electromagnetic particle-in-cell simulations,[21] the plasma is treated as a set of marker particles interacting with each other through self-generated electromagnetic fields. Electrostatic potential is solved by gyrokinetic Poisson equation, and magnetic vector potential is solved by Ampere's law. For simulations presented in this paper, we use gyrokinetic equations to deal with ion dynamics, which is valid for the edge parameters.[6] Drift kinetic equation is used for electron dynamics because of its small gyro-radius. An electromagnetic fluid-kinetic hybrid model[21,22] based on the expansion of the electron response into adiabatic and non-adiabatic parts is employed for electrons instead of the drift-kinetic model to avoid numerical constrains introduced by electron drift kinetic equations. To reduce particle noise, we use the δf method to solve for perturbed gyrocenter distribution functions. The perturbed field quantities are zero at both sides of radial boundary and periodic in poloidal and toroidal directions. Note that the free-boundary condition would allow a finite amplitude of the perturbation of the instability at the radial boundary, which is important for the peeling-ballooning mode. Collision operators conserving momentum and energy are also implemented in GTC, with the pitch angle scattering operator for electron-ion collisions and Fokker-Planck operator for like-species collisions.[23]

The plasma equilibrium is based on DIII-D discharge 145701 at time 33 ms, as seen in Fig. 1. To identify local instabilities in the peak gradient region, our simulation domain includes the whole pedestal with the normalized poloidal magnetic flux ψ_n from 0.9 to 1.0 (normalized by its value at the separatrix). Density, temperature, and their gradients are constant values in the whole simulation domain (analogous to the uniform loading scheme in Ref. 24), which are taken from a local point at $\psi_n = 0.984$ in the peak gradient region, seen as the vertical dashed line in Fig. 1. Full q-profile and realistic non-circular, up-down asymmetric magnetic geometry from VMEC reconstruction[20] are used. The parameters in the steep gradient region are: electron temperature $T_e = 197\,\mathrm{eV}$, ion temperature $T_i = 396\,\mathrm{eV}$, density $n_e = n_i = 2.48 \times 10^{13}\,\mathrm{cm}^{-3}$, and their gradients $R_0/L_{T_e} \approx 144$, $R_0/L_{T_i} \approx 8$, $R_0/L_n \approx 64$, $\eta_i = L_n/L_{T_i} \approx 0.13$, and $\eta_e \approx 2.25$. The scale length L_f for a radial function $f(r)$ is defined by $L_f^{-1} = \mathrm{d}\ln f(r)/\mathrm{d}r$. Safety factor is $q = 3.6$ and β_e is around 0.07%, where $\beta_e = 8\pi n_e T_e / B_0^2$. The total plasma β is defined as $\beta = \beta_e + \beta_i$. Other parameters are: the major radius $R_0 = 1.77\,\mathrm{m}$, the aspect ratio $\varepsilon = a/R_0 = 0.37$, where a is the minor radius of the tokamak, the toroidal magnetic field $B_0 = 1.68\,\mathrm{T}$, and the deuterium to electron mass ratio $m_D/m_e = 3672$. Collisions with effective charge number $Z_{eff} = 1.5$ are also included in our simulation since collisional effects may be important in edge plasmas with relatively low temperature. The present global simulations focus on the study of the properties of electromagnetic modes. The comparison with local gyrokinetic simulation results should be carefully done in the future, since KBM is very sensitive to equilibrium, physics model, and boundary conditions.

III. SIMULATION RESULTS

All the linear results presented in this paper are from simulations of a single toroidal mode number n, due to toroidal symmetry. To identify the most unstable mode in the peak gradient region, we first use a higher $\beta_e = 0.14\%$ at the inner part of the pedestal, shown in panel 3 of Fig. 1. The dependence of linear growth rate and frequency on n is shown in Fig. 2. We can see two branches of instabilities: one propagates in the ion diamagnetic direction (negative real frequency) and the other is in the electron diamagnetic direction (positive real frequency). We identify the lower-n ($n \leq 25$) branch as KBM and the higher-n branch ($n > 30$) as TEM according to their propagation direction, mode structure, and growth rate dependence on β_e, and electron kinetic effects. KBM is insensitive to electron kinetic effects and still unstable even when electrons are treated as a massless

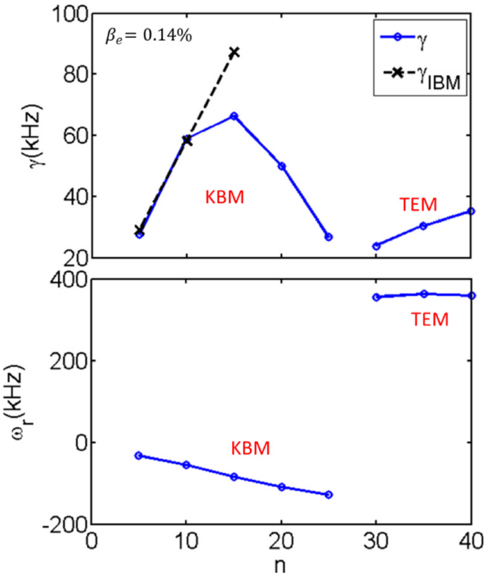

FIG. 2. Toroidal mode number n dependence of the linear growth rate (top panel) and real frequency (bottom panel) using $\beta_e = 0.14\%$. The γ_{IBM} in the top panel is the ideal ballooning mode drive defined as $\gamma_{\mathrm{IBM}} = k_\theta \rho_e v_{the}/\sqrt{R_0 L_n}$.

fluid. TEM can be observed only when we use kinetic electron model in both electromagnetic and electrostatic simulations. The results presented in this paper are qualitative and can partially verify the EPED model (KBM is the most unstable mode in the pedestal recovery stage).[15] The growth rate of the KBM peaks at $n = 15$, and the growth rate of the TEM increases with n. The frequency of the KBM is around 100 kHz in the plasma frame, and the poloidal wave number for $n = 15$ is $k_\theta \rho_i = 0.15$, which is consistent with DIII-D experimental results.[25] The TEM has a higher frequency around 350 kHz. The growth rate of the low-n KBM is compared to the ideal ballooning mode drive $\gamma_{\mathrm{IBM}} = k_\theta \rho_e v_{the}/\sqrt{R_0 L_n}$ as shown in Fig. 2. We see that the ideal MHD growth rate is a good approximation to the KBM growth rate for low-n modes ($n \leq 10$), but is inaccurate for high-n modes of $n > 10$. The diamagnetic drift frequency defined as $\omega^* = k_\theta \rho_e v_{the}/L_n$ is much larger than the real frequency.

Poloidal mode structures of the electrostatic potential and parallel vector potential of these two branches are quite different as shown in Fig. 3. The KBM has a typical ballooning structure peaking at the outer mid-plane, which is in contrast with the unconventional mode structure of the KBM in helical plasmas.[26] The mode structure of the TEM peaks at the top and bottom of the poloidal plane because of the steep pressure gradient. The unconventional mode structures are similar to those reported by the electrostatic simulations in Refs. 6 and 7 and can possibly be explained by the eigenstates transition or non-zero ballooning angle theories in Refs. 7 and 27. The radial profiles of the electrostatic potential for the poloidal harmonics are also shown in Fig. 3. We can see that for the TEM with unconventional mode structure, the spectra of neighboring poloidal numbers have the opposite phase $\phi_m \simeq -\phi_{m+1}$, which leads to the destructive interference at the outer mid-plane. On the other hand, the phase between neighboring poloidal numbers $\phi_m \simeq \phi_{m+1}$ is the same for the KBM with the conventional mode structure. The unconventional structure with the opposite phase of neighboring poloidal harmonics has also been observed in HL-2A edge electrostatic simulation in Ref. 7.

To find the critical β_e threshold for the KBM instability, we keep a constant toroidal number n and scan β_e by changing the electron density while keeping the gradient $\mathrm{d}\ln n_e/\mathrm{d}\psi_n$ unchanged. For $n = 40$, the dependence of linear growth rate and frequency on β_e is shown in Fig. 4. We can see that the TEM is the most unstable instability at low β_e. The growth rate of the TEM is independent of β_e since parallel electric field has little effects on trapped electrons, in contrast to the familiar β-stabilization of the ITG mode in earlier simulations.[19] As β_e increases to around 0.35%, the KBM takes over the TEM to be the dominant instability with an estimated stability threshold at $\beta_e \approx 0.28\%$, and its growth rate increases monotonically with β_e. Also, KBM has a conventional mode structure with electrostatic potential peaking at $\theta = 0$, while the TEM mode structure peaks at $\theta \sim \pm\pi/2$. Collisions with an effective charge number $Z_{eff} = 1.5$ are considered in this case. The effective collision frequency for electron-electron collision is $\nu_e^* = 0.58$ and the ion-ion collision is $\nu_i^* = 0.16$. Here, the effective collision frequency is

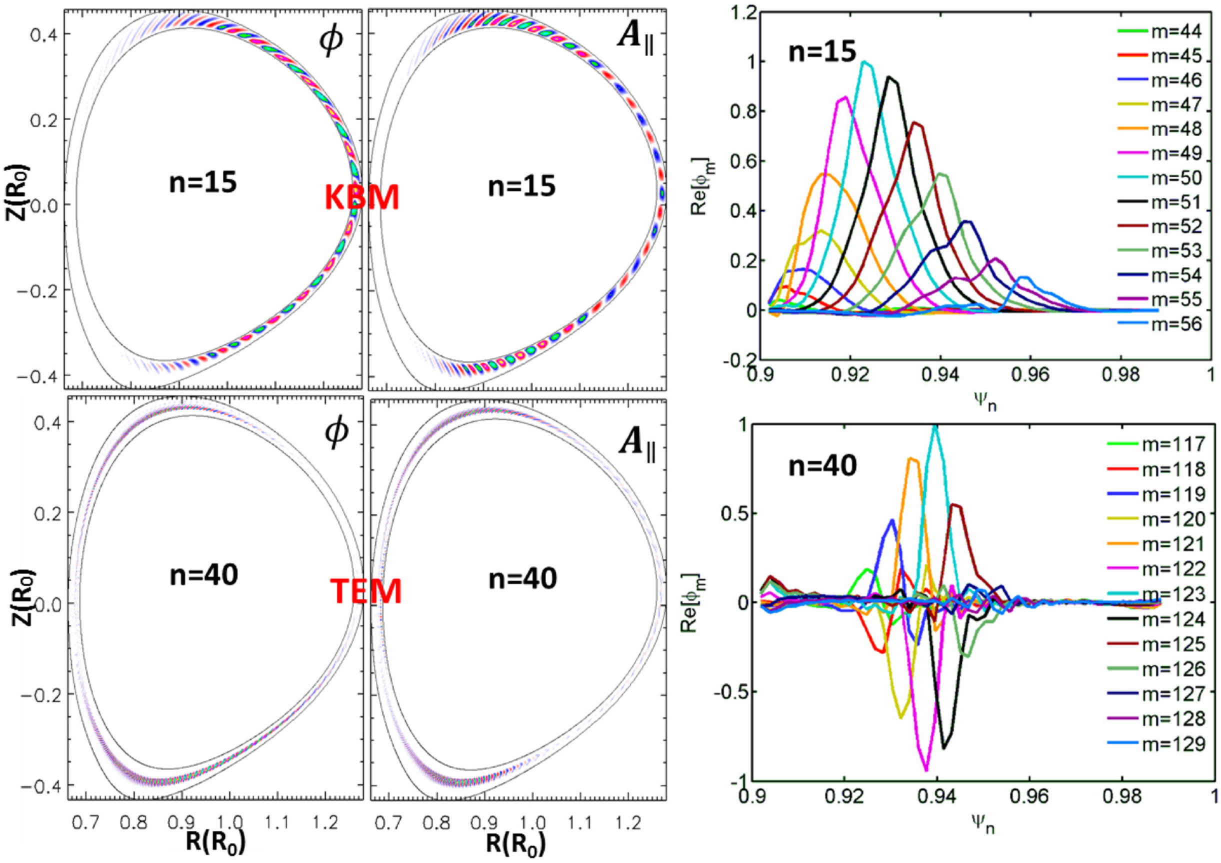

FIG. 3. The poloidal structure of electrostatic potential (ϕ) and parallel vector potential ($A_{||}$) of $n = 15$ (top panel, KBM) and $n = 40$ (bottom panel, TEM) using $\beta_e = 0.14\%$ (left columns) and radial profiles of the electrostatic potential for the poloidal mode numbers (right columns).

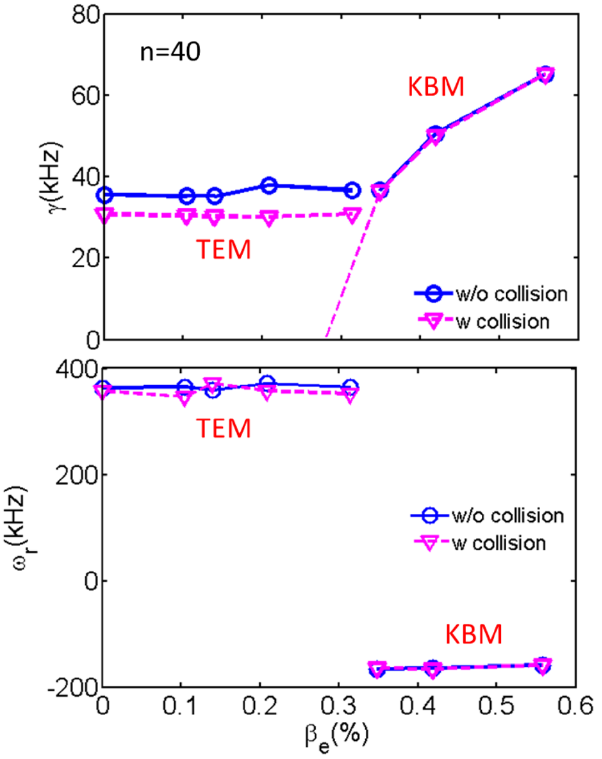

FIG. 4. β_e dependence of the linear growth rate (top panel) and real frequency (bottom panel) of $n = 40$ mode in the peak gradient region.

defined as $\nu^* = \varepsilon^{-3/2}\nu\sqrt{2}qR_0/v_{th}$, and $v_{th} = \sqrt{T/m}$ is the thermal velocity. The results are also shown in Fig. 4. We can see that collisions reduce the TEM growth rate by about 15%, while have little effects on the growth rate of KBM. This is due to the larger collision frequency for trapped electron, which is the main drive for the TEM, and the smaller collision frequency for ion, which is the main drive for the KBM.

For a lower toroidal mode number $n = 15$, where KBM has the maximal growth rate, the β_e dependence of the linear growth rate and real frequency is shown in Fig. 5. We can see that the transition from TEM to KBM is at $\beta_e \approx 0.09\%$, within the range of the pedestal region ($\beta_e < 0.2\%$). The KBM stability threshold can be estimated at $\beta_e \approx 0.07\%$ from the top panel of Fig. 5. For a higher toroidal mode number n, the TEM-KBM transition occurs at a higher β_e, since KBM is linearly stabilized at the higher toroidal mode numbers, while the TEM growth rate depends monotonously on n for the low-n modes. A purely growing mode (with zero frequency) is observed when we take the ideal MHD limit (using only electron fluid model[28]) for this case, as shown in Fig. 5. This zero frequency mode is the ideal ballooning mode, which was predicted by local ballooning mode theory and has an identical critical pressure value (and its gradient) to that for the KBM at $\eta_i = 0$ limit.[29] In our simulations, the total plasma $\beta = \beta_e + \beta_i$ and $\beta_i = 2.02\beta_e$ for the KBM simulations, but $\beta_i = 0$ for the IBM simulations, which gives stability threshold $\beta_c^{\mathrm{KBM}} \approx 1.9\beta_c^{\mathrm{IBM}}$. However, the ballooning mode is mainly driven by the pressure gradient, which is $\beta_c'^{\mathrm{KBM}} \approx \beta_c'^{\mathrm{IBM}}$, i.e., the critical pressure gradient for the KBM is similar to that for the IBM. This result agrees with the local theory at $\eta_i = 0$ limit.[29] Furthermore, collisions are not important for the KBM, as shown in Fig. 5. Mode structures of the KBM and IBM at $\beta_e = 0.14\%$ are shown in Fig. 6. The IBM has a conventional mode structure similar to that for the KBM, with electrostatic potential peaking at $\theta = 0$.

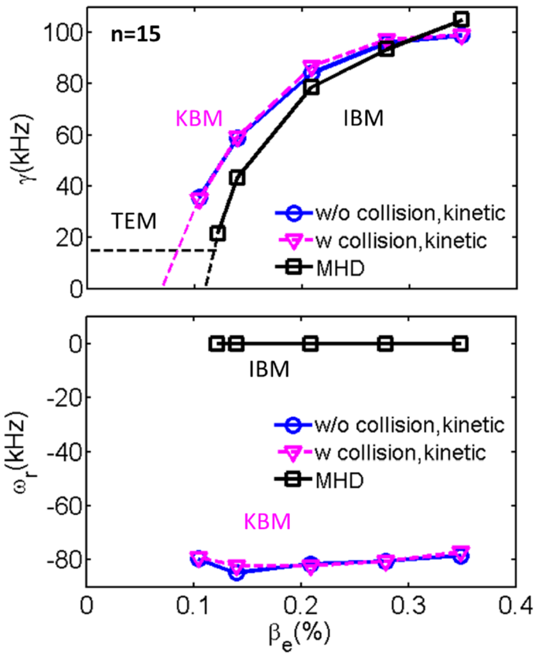

FIG. 5. β_e dependence of the linear growth rate (top panel) and real frequency (bottom panel) of $n = 15$ instability in the peak gradient region. The dashed horizontal line for the TEM growth rate is from an electrostatic simulation.

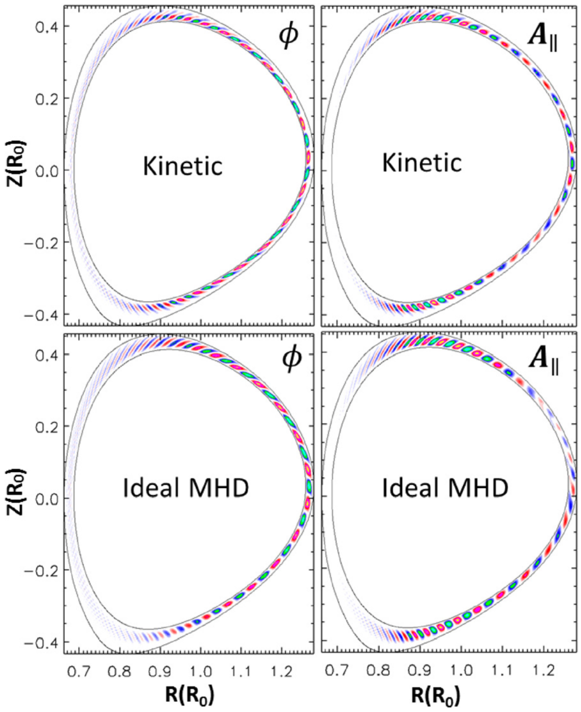

FIG. 6. The poloidal structure of electrostatic potential (ϕ) and parallel vector potential ($A_\parallel$) of $n = 15$ mode in kinetic simulation (the top panel) and ideal MHD simulation (the bottom panel).

IV. CONCLUSION AND DISCUSSION

In this study, gyrokinetic simulations of electromagnetic instabilities have been carried out with real tokamak geometry and local parameters taking from the steep gradient region in the pedestal of DIII-D experiments. We find that the kinetic ballooning mode (KBM), which has a conventional mode structure peaking at the poloidal angle $\theta = 0$, is the dominant instability for moderate toroidal mode numbers ($n \leq 25$). For larger toroidal mode numbers ($n > 30$), the most unstable mode is the trapped electron mode (TEM), which has an unconventional mode structure peaking at $\theta \sim \pm\pi/2$. We observe a KBM-TEM transition by increasing toroidal mode number at a fixed plasma pressure or by increasing plasma pressure with a fixed toroidal mode number. For a higher n, the transition from TEM to KBM occurs at a higher pressure. The ideal ballooning mode is also observed when we take the ideal MHD limit, which has a similar threshold of the pressure gradient to that for the KBM. Collisions slightly damp the TEM and have little effects on the growth rate of the KBM. The toroidal mode number and frequency range of the KBM are consistent with DIII-D experimental observation. To fully understand edge instabilities and quantitatively compare with experimental results, more realistic global simulations should be carried out with full plasma profiles and equilibrium radial electric fields as well as the nonlinear effects.

ACKNOWLEDGMENTS

The authors would like to thank useful discussions with W. L. Zhang, H. S. Xie, J. Bao, and GTC Team. This work was supported by ITER-China Program (Grant Nos. 2013GB111000 and 2013GB112006), National Natural Science Foundation of China (Grant No. 11275162), and U.S. DOE theory Grant No. DE-SC0010416. This research used resources of the Oak Ridge Leadership Computing Facility at Oak Ridge National Laboratory (DOE Contract No. DE-AC05-00OR22725), and the National Energy Research Scientific Computing Center (DOE Contract No. DE-AC02-05CH11231), and the National Supercomputing Center in Tianjin.

[1] F. Wagner, G. Becker, K. Behringer, D. Campbell, A. Eberhagen, W. Engelhardt, G. Fussmann, O. Gehre, J. Gernhardt, G. v. Gierke, G. Haas, M. Huang, F. Karger, M. Keilhacker, O. Klüber, M. Kornherr, K. Lackner, G. Lisitano, G. G. Lister, H. M. Mayer, D. Meisel, E. R. Müller, H. Murmann, H. Niedermeyer, W. Poschenrieder, H. Rapp, H. Röhr, F. Schneider, G. Siller, E. Speth, A. Stäbler, K. H. Steuer, G. Venus, O. Vollmer, and Z. Yü, Phys. Rev. Lett. **49**(19), 1408–1412 (1982).

[2] J. M. Canik, R. Maingi, S. Kubota, Y. Ren, R. E. Bell, J. D. Callen, W. Guttenfelder, H. W. Kugel, B. P. LeBlanc, T. H. Osborne, and V. A. Soukhanovskii, Phys. Plasmas **18**(5), 056118 (2011).

[3] J. M. Canik, W. Guttenfelder, R. Maingi, T. H. Osborne, S. Kubota, Y. Ren, R. E. Bell, H. W. Kugel, B. P. LeBlanc, and V. A. Souhkanovskii, Nucl. Fusion **53**(11), 113016 (2013).

[4] E. Wang, X. Xu, J. Candy, R. J. Groebner, P. B. Snyder, Y. Chen, S. E. Parker, W. Wan, G. Lu, and J. Q. Dong, Nucl. Fusion **52**(10), 103015 (2012).

[5] F. Liu, Z. Lin, J. Q. Dong, and K. J. Zhao, Phys. Plasmas **17**(11), 112318 (2010).

[6] D. P. Fulton, Z. Lin, I. Holod, and Y. Xiao, Phys. Plasmas **21**(4), 042110 (2014).

[7] H. Xie and Y. Xiao, Phys. Plasmas **22**(9), 090703 (2015).

[8] W. Wan, S. E. Parker, Y. Chen, R. J. Groebner, Z. Yan, A. Y. Pankin, and S. E. Kruger, Phys. Plasmas **20**(5), 055902 (2013).

[9] D. Dickinson, S. Saarelma, R. Scannell, A. Kirk, C. M. Roach, and H. R. Wilson, Plasma Phys. Controlled Fusion **53**(11), 115010 (2011).

[10] J. W. Connor, R. J. Hastie, H. R. Wilson, and R. L. Miller, Phys. Plasmas **5**(7), 2687 (1998).

[11] P. T. Lang, G. D. Conway, T. Eich, L. Fattorini, O. Gruber, S. Günter, L. D. Horton, S. Kalvin, A. Kallenbach, M. Kaufmann, G. Kocsis, A. Lorenz, M. E. Manso, M. Maraschek, V. Mertens, J. Neuhauser, I. Nunes, W. Schneider, W. Suttrop, H. Urano, and ASDEX Upgrade Team, Nucl. Fusion **44**(5), 665–677 (2004).

[12] P. B. Snyder, H. R. Wilson, J. R. Ferron, L. L. Lao, A. W. Leonard, T. H. Osborne, A. D. Turnbull, D. Mossessian, M. Murakami, and X. Q. Xu, Phys. Plasmas **9**(5), 2037 (2002).

[13] S. J. Fielding, P. G. Carolan, J. W. Connor, N. J. Conway, A. R. Field, P. Helander, Y. Igitkhanov, B. Lloyd, H. Meyer, A. W. Morris, O. Pogutse, M. Valovic, and H. R. Wilson, Nucl. Fusion **41**(7), 909 (2001).

[14] H. R. Wilson, P. B. Snyder, G. T. A. Huysmans, and R. L. Miller, Phys. Plasmas **9**(4), 1277 (2002).

[15] P. B. Snyder, R. J. Groebner, A. W. Leonard, T. H. Osborne, and H. R. Wilson, Phys. Plasmas **16**(5), 056118 (2009).

[16] Z. Lin, T. S. Hahm, W. W. Lee, W. M. Tang, and R. B. White, Science **281**, 1835 (1998).

[17] W. Zhang, Z. Lin, and L. Chen, Phys. Rev. Lett. **101**(9), 095001 (2008).

[18] Y. Xiao and Z. Lin, Phys. Rev. Lett. **103**(8), 085004 (2009).

[19] I. Holod, D. Fulton, and Z. Lin, Nucl. Fusion **55**(9), 093020 (2015).

[20] S. P. Hirshman and J. C. Whitson, Phys. Fluids **26**(12), 3553 (1983).

[21] I. Holod, W. L. Zhang, Y. Xiao, and Z. Lin, Phys. Plasmas **16**(12), 122307 (2009).

[22] Z. Lin and L. Chen, Phys. Plasmas **8**(5), 1447 (2001).

[23] Z. Lin, W. M. Tang, and W. W. Lee, Phys. Plasmas **2**(8), 2975 (1995).

[24] Y. Xiao, I. Holod, Z. Wang, Z. Lin, and T. Zhang, Phys. Plasmas **22**(2), 022516 (2015).

[25] Z. Yan, G. R. McKee, R. J. Groebner, P. B. Snyder, T. H. Osborne, and K. H. Burrell, Phys. Rev. Lett. **107**(5), 055004 (2011).

[26] A. Ishizawa, T. H. Watanabe, H. Sugama, S. Maeyama, and N. Nakajima, Phys. Plasmas **21**(5), 055905 (2014).

[27] T. Xie, Y. Z. Zhang, S. M. Mahajan, and A. K. Wang, Phys. Plasmas **19**(7), 072105 (2012).

[28] Z. Li, G. Sun, I. Holod, Y. Xiao, W. Zhang, and Z. Lin, Plasma Sci. Technol. **15**(6), 499–505 (2013).

[29] C. Z. Cheng, Phys. Fluids **25**(6), 1020 (1982).